PROCEEDINGS, 42nd Workshop on Geothermal Reservoir Engineering
Stanford University, Stanford, California, February 13-15, 2017
SGP-TR-212

Geomechanics-Based Stochastic Analysis of Microseismicity for Analysis of Fractured Reservoir Stimulation

Jianrong Lu, Ahmad Ghassemi

Reservoir Geomechanics and Seismicity Research Group, the University of Oklahoma, Norman, OK

ahmad.ghassemi@ou.edu

Keywords: Fracture Network Characterization, Induced Microseismicity, Similarity Measure, Mahalanobis Distance, Poroelasticity

ABSTRACT

Natural fractures are the primary pathways for fluid migration and production in unconventional geothermal and petroleum reservoirs. In geothermal reservoirs, reactivation (and possible propagation) of natural fractures is an important component of stimulation. Slip on these fractures induced Microearthquakes (MEQs) and the locations of MEQ events reveal aspects of stimulation. In this paper, we discuss a technique for extracting information about fractures orientations from MEQs. This is achieved by combining geomechanics and geostatistics to better constrain uncertainties in natural fracture properties. We develop a new Geomechanics-Based Stochastic Analysis of Microseismicity (GBSAM) to provide quantitative estimate of fractures orientations. In this work, the rock response to pore pressure is modeled using a line injection source to simulate water injection into a natural fracture network. Mahalanobis distance is then used to quantify the similarity between the distribution of MEQs (GMEQs) from the forward model and field-observed distribution of MEQs (TMEQs) to find the best GMEQs that fits the TMEQs. As an example, the GBSAM is applied to a data set of 494 MEQs recorded during phase 2.1 and 2.2 of Newberry Volcano EGS demonstration project, located 37 km south of Bend, Oregon. Borehole televiewer (BHTV) was used successfully to map the geometry of 351 fractures in the wellbore. Results from GBSAM show that there are two sets of fractures in Newberry reservoir with dip of 63^o and dip of 56^o. The dip of those fractures have good agreement with the field results from BHTV. This proposed method provides an effective and general way for interpreting MEQs for better characterizing reservoir stimulation.

1. INTRODUCTION

The geometry of fractures has a significant impact on the fluid flowing, thermal transport capabilities and mechanical stability of a rock mass. Fractures orientations, spacing, connectivity are important features that control network permeability. Despite their essential role in reservoir development, there still are uncertainties regarding direct and indirect diagnostic technologies for characterizing fractures orientations in in-situ environments is not well developed. In the last several decades, many methods have been used to constrain the uncertainty in measuring the fractures orientations. Borehole logging and camera and outcrop mapping are commonly suffered from lower dimensional limited exposures (Einstein and Baecher 1983, Williams and Johnson 2004, Li, Feng et al. 2013). Furthermore, the description of fracture geometries obtained from local field surveys has to upscale from the local scale to the entire reservoir which can cause loss of geometric characteristics of the fractures. The question of how to establish reliable a fracture pattern remain an unresolved issue in subsurface community. Thus, fracture pattern in numerical analysis are commonly treated in a stochastic framework (Leung and Zimmerman 2012, Berrone, Pieraccini et al. 2015, Farmahini-Farahani and Ghassemi 2015, Ghassemi and Tao 2016).

Cold water injection perturbs the pore pressure and the in-situ stress state within the reservoir leading to fracture initiation and/or activation of discontinuities such as faults and fractures which is often manifested as multiple MEQs. Detection and interpretation of MEQs using downhole receiver arrays (Brady, Withers et al. 1994, Warpinski, Wright et al. 1999) can be analyzed to provide useful information on the stimulated zone, created reservoir permeability and fracture growth, and geometry of the geological structures and the in-situ stress state(Pine and Batchelor 1984, Gutierrez-Negrin and Quijano-Leon 2003, Warpinski, Wolhart et al. 2004) MEQs are believed to be associated with rock failure in shear, and shear slip on new or pre-existing fracture planes (Pearson 1981). The generated MEQs contain information about the sources of energy that can be used for understanding the hydraulic fracturing process (Talebi, Young et al. 1991, Shapiro, Huenges et al. 1997, Foulger, Julian et al. 2004) and the created reservoir properties. The growth of the fractured zone direction can be determined using inverse modeling of micro-seismic observations. This inverse modeling is commonly referred to as seismicity based reservoir characterization (SBRC) and can been used to estimate the rock mass permeability tensor resulting from stimulation(Shapiro, Patzig et al. 2003). In the premier works (Shapiro, Huenges et al. 1997), a diagnostic technique is developed to estimate the crust permeability from MEQs. Pore pressure diffusion model is used to link MEQs to equivalent permeability at reservoir scale and the crust is assumed in the failure equilibrium. Therefor GMEQs will generate when the beginning of the injection. The hydraulic diffusivity can be determined when the diffusion length-time curve fit for the onset of seismicity. This approach is very simple and but lack quantitative analysis between the TMEQs and GMEQs. This framework was further improved by combining geomechanics model and ensemble Kalman filter (EnKF) to infer reservoir permeability and geomechanical property from MEQs as part of our DOE-funded research(Ghassemi 2012, Tarrahi and Jafarpour 2012, Ghassemi 2013, Tarrahi, Jafarpour et al. 2015). Kernel density estimation (KDE) was used to smooth MEQs as continue seismicity density since most inversion algorithms (e.g. EnKF) are designed to integrate continuous data. However, a noticeable limitation of KDE is that it cannot capture the discrete natural of MEQs and the value of discrete MEQs is compromised. There are also several limitations for the KnEF used as tool for interpreting MEQs, including (a) EnKF used in large data results in sever ensemble spread underestimation. (b) EnKF can only handle continuous data and MEQs is a type of discrete data. (c) EnKF cannot handle high nonlinear relation between the flow data and unknown

parameters results hardly converged. Fractures surface roughness is recommend to link the magnitude of a MEQs to fracture permeability change based on empirical formulas (Ishibashi, Watanabe et al. 2016).

Other traditional MEQs interpretations have relied on grouping MEQs based on the graph operations which rely on the locations of the MEQs hypocenters (Fehler, House et al. 1987, Fehler and Johnson 1989, Fehler 1990, Jones and Stewart 1997). Another type of approach is to first group the MEQs with similar waveform (e.g., focal mechanisms, ratio of S wave to P wave amplitudes) and then search for self-similar MEQs clusters to define the fractures (Aster and Scott 1993, Roff, Phillips et al. 1996, Kuang, Zoback et al. 2017). So the sets of clusters are grouped into planar and fault plane can be defined as the best fit for ach cluster. The concept of measure similarity was the first to apply to distinguish different MEQs based on the objective function depending on the ratio of S wave to P wave amplitudes and maximum separation distance(Roff, Phillips et al. 1996). The concept of similarity measure was also used but with four-term objective function that becomes much more complex(Kuang, Zoback et al. 2017). In these approaches, the focal mechanism solution with the largest value of objective function is most likely to be the best. However, due to arbitrariness of the objective function and low magnitude of MEQs, this method seem to be poorly constrained and contains large errors. Furthermore, these methods suffers from three limitations: 1. the objective function is complex resulting in convergence difficulties; 2. Waveform of MEQs is probably disorganized and amplitude is very low, so only very strong MEQs can be selected; 3. There is no general theoretical framework to quantitatively measure the matching level between the MEQs.

In this work we develop an alternative method that can help characterize the fracture population in the reservoir. Similarity measure is a real-valued function that quantifies the similarity between two objects(Jarvis and Patrick 1973, Frey and Dueck 2007). The core of similarity measure is to build the distance metrics between the two object, for instance, the distance metrics is calculated from the center of one object to center of another object. In this study, we use this approach to develop a stochastic framework called Geomechanics-Based Stochastic Analysis of Microseismicity (GBSAM) to integrate TMEQs as prior information to infer fractures orientations. MEQs are generated when the shear stress at the center of fractures are larger than the shear strength according to the Mohr-Coulomb failure criterion. If the stored strain energy is larger than the threshold energy of MEQs, additional MEQs are generated on the fracture plane stochastically. Mahalanobis distance is then applied to measure the similarity between TMEQs and GMEQs (Huberty 2005). The uniqueness and existential of solution from GBSAM also has been investigated. Finally, the GBSAM is applied to a data set of MEQs recorded during phase 2.1 and 2.2 of Newberry Volcano EGS demonstration project, located 37 km south of Bend, Oregon.

2. POROELASTIC MODELING OF INJECTION AND MEQS GENERATION

Water injection will disturb the initial pore pressure and stress fields in the reservoir and fractures are reactivated and potentially induce MEQs. This configurations can be approximate via a line injection source in horizontal permeable zone which is bounded by two semi-infinite impermeable zones (Figure 1). The line injection source $(r = 0)$ extends over the thickness of the permeable layer and injects fluid into the surrounding rock masses at a constant volumetric rate Q. The shear modulus G and Poisson's ratio v and other poroelastic constants are pre-identified (Table 1). The fractures are stochastically distributed throughout the permeable zone which is assigned an effective permeability. Thermal effects are neglected in this study. Initially $(t = 0)$, all the hydraulic and mechanical fields are assumed to be in equilibrium state.

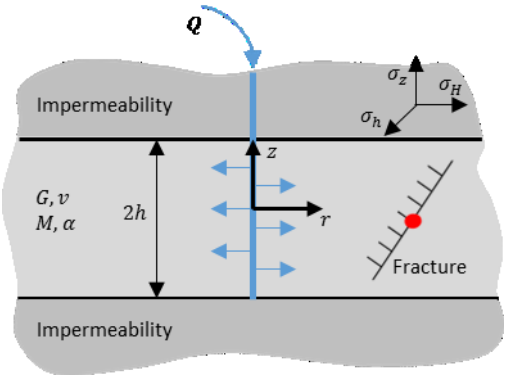

Figure 1: Geometry of the problem: a line injection source with fractures in permeability layer. The red point is the center of the fracture

To drive the analytical pore pressure solutions for uniformity of line source density over the thickness of the reservoir injection into an infinite homogeneous poroelastic medium, the diffusion equation can be obtained from Biot theory:

$$\frac{\partial p}{\partial t} = c\nabla^2 p \tag{1}$$

Where p is the pore pressure. c is the diffusivity coefficient defined by as follow: $c = 2\kappa G(1-v)(v_u - v)/\left(\alpha^2(1-2v)^2(1-v_u)\right)$. Here κ is the permeability coefficient, α is the Biot coefficient, G is the shear modulus, v is the drained Poisson's ratio and v_u is undrained Poisson's ratio.

The diffusion equation (1) can be solved together with the initial condition ($p = 0\ at\ t = 0,\ 0 < r < \infty$) and boundary conditions($p = 0\ at\ r = \infty\ and\ t > 0$). The solution of the pore pressure diffusion equation (1) with the stated initial and boundary conditions is a classic similarity solution:

$$p = \frac{Q}{8 \cdot \pi \kappa h} \int_r^{\infty} \frac{e^{-\tau}}{\tau} \mathrm{d}\tau \cdot \left(\frac{r^2}{4Dt}\right) \tag{2}$$

From solution (2), the effective stress $\sigma'$is equal to $\sigma - p$. Here σ is the total stress. To computer shear and normal stress, one must specify the definition of fracture orientation (Figure 2 (a)).

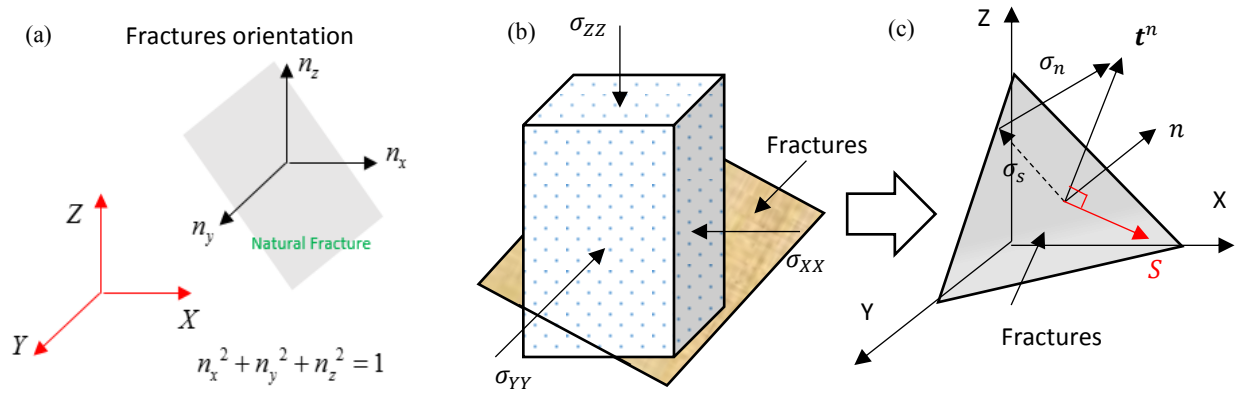

Figure 2: Geometry of the fracture: (a) fracture orientation and (b), (c) stress field on the fracture

In order to calculate the effective normal stress σ_n and shear stress σ_s acting on arbitrary plane whose unit normal is $[n_x, n_y, n_z]$ at the center of fracture (red point in figure 1). From the Cauchy's law, the traction vector $\boldsymbol{t}^n$on fracture is $\sigma'_{ij} n_j, \sigma'_{ij}$ is the effective stress. The normal stress to the fracture is $\sigma_n = \boldsymbol{t}^n \cdot n$ and shear stress σ_s is $\sqrt{|\boldsymbol{t}^n|^2 - \sigma_n^2}$. The slip direction of fracture S is $\left[\frac{\sigma_1 - \sigma_n}{\sigma_s} n_x, \frac{\sigma_2 - \sigma_n}{\sigma_s} n_y, \frac{\sigma_3 - \sigma_n}{\sigma_s} n_z\right]$. The Coulomb failure function (CFF) which describes the proximity of fracture to frictional slipping and is formulated as

$$\mathrm{CFF} = \sigma_s - \mu \sigma_n - C \tag{3}$$

Where μ is the friction coefficient and C is the cohesive strength. One essential limitation in this method is that mechanics field on the fracture plane is slightly difference between each other. Analytical models hardly capture such details of the fracture plane. So in this study, the geometry of fracture is treated as a mass point located on the center of fracture (Figure 3(a)). The mass point inherit all the geometrical and mechanics properties of the fracture. So the mechanics field of the mass point represent the mechanics state of entire fracture. Another essential limitation in the current formulation is that if any physical point (element) on the fracture is fail, one GMEQs will be generated. Recently, different numerical methods such as discrete element method (Zhao and Paul Young 2011, Khazaei, Hazzard et al. 2016), hybrid boundary element/finite element(Safari and Ghassemi 2016) are applied to simulate MEQs. However these methods do not consider the analysis of wave generation and propagation at frictional sliding interfaces. A fracture plane can have multiple MEQs and usually some re-defined heuristics are used to control the number of MEQs. From this aspect, numerical methods do not necessarily provide a significant advantage. Due to the scale mismatch between physical point (element) and fracture, we propose a new method to outline the location and the number of GMEQs that will be generated on a fracture plane. If CFF is large than zero and the fracture is slipping, a GMEQs will be occurred at the center of fracture. In this configuration, the stored shear strain energy of fracture is calculated. A certain part of stored shear strain energy in the contact surface is released in the form of seismic wave during the fracture slipping processes. If the seismic energy is larger than the pre-defined threshold energy of MEQs, additional GMEQs will be generated (Figure 3(b)). Specially, the location of additional GMEQs are randomly distributed on the fracture plane. The threshold energy of MEQs is pre-defined based on the estimation in this study. The seismic energy from P and S waves can be estimated following (Boatwright and Fletcher 1984)

$$E_c = 4\pi \rho V_c \langle F_c \rangle^2 \left(\frac{R}{F_c R_c}\right)^2 J_c \tag{4}$$

Where E_c is the seismic energy and J_c is the energy flux, ρ is the rock density and F_c is the average P or S wave radiation coefficient. R is the source-receiver distance, V_c is the body wave velocity. The seismic energy can be calculated based on the experiment results(Goodfellow and Young 2014). So the threshold energy of MEQs is assumed to the same as the average the seismic energy E_c.

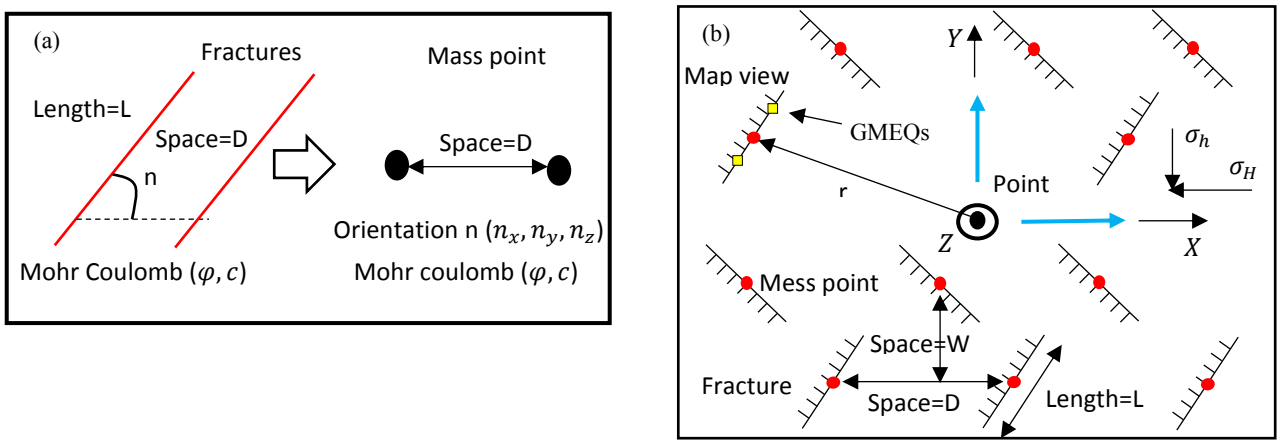

Figure 3: Assumption in GBSAM: (a) mass point assumption and (b) additional GMEQs assumption

3. MAHALANOBIS DISTANCE

The concept of similarity is essential to the pattern recognition problems and is applied on the data classification and clustering in data sciences (Cha 2007). From the data scientist's perspective, similarity is defined as a quantitative degree of how far apart are two discrete or continuous objects. Hence, the concept of similarity is appropriate for measuring the matching level between the GMEQs and TMEQs. The fracture orientation in the forward model with the smallest value of similarity is most likely to be the best and is considered to be the same as the true fracture orientation in the reservoir. Here, the Mahalanobis distance (MD), a concept of similarity, is used to quantify the matching level between GMEQs and TMEQs. MD is defined on both the mean and variance of the predictor variables and the covariance matrix of all the variables, and therefore it takes advantage of the covariance among variables. For instance, suppose we have two data groups of MEQs and they are all two dimensional. Data group 1 is $X(x_i^1, x_i^2)$ and Data group 2 is $Y(y_j^1, y_j^2)$. The number of MEQs in each group may not be the same $(i \neq j)$. The center of each data group can be calculated as $X - mean(X)$ and $Y - mean(Y)$ respectively. In the next step, we center these two data groups on the arithmetic mean of each variable as follow:

$$S_1 = \frac{1}{n_1}\bar{X}\bar{X}^T = \frac{1}{n_1}[x^1\ x^2\ ]\begin{bmatrix}x^1\\x^2\end{bmatrix} \text{ and } S_2 = \frac{1}{n_2}\bar{Y}\bar{Y}^T = \frac{1}{n_2}[y^1\ y^2\ ]\begin{bmatrix}y^1\\y^2\end{bmatrix} \tag{5}$$

Where n_1 and n_2 is the number of data in group 1 and group 2, respectively. The covariance matrix of each group is computed using the centered data matrix. The pooled covariance matrix of two data groups is computed as weighted average of the covariance matrices as follow:

$$S = \frac{n_1}{n_1+n_2}S_1 + \frac{n_2}{n_1+n_2}S_2 \tag{6}$$

The value of MD is simply quadratic multiplication of mean difference and inverse of pooled covariance matrix.

$$d(X,Y) = \sqrt{(\bar{X}-\bar{Y})^T S^{-1}(\bar{X}-\bar{Y})} \tag{7}$$

4. PROCEDURES FOR THE GBSAM ANALYSIS

Suppose a 3D reservoir with unknown fracture orientation $n = \{n_x, n_y, n_z\}$ and the goal is to identify its unknown fracture orientation by performing inverse analysis. Since it is difficult to determine all of the three components of fracture orientation from a highly uncertain reservoir system, some necessary assumptions are made. The locations of fractures are assumed to be the same as the TMEQs. The shape of the fractures is penny and the radius is a pre-defined constant and thus the direction component n_x is assumed to be a constant. The parameters in the line source model are also assumed to be known (Cheng and Ghassemi 2016). The orientation of individual fractures is randomly allocated and then the fracture population is equally divided into two sets in random form in every cycle. To interpret TMEQs for fracture orientation we propose a general inverse analysis named GBSAM. These assumptions preserve the GBSAM characteristics while optimizing the inverse analysis. Here we need to point out that GBSAM cannot predicate orientation of each individual fracture and it only provides the likely orientation of each set.

The procedures of the computational algorithm for extracting fractures orientation from TMEQs, plus an additional converged analysis are reported (Lu and Ghassemi 2017). One need to check whether the GBSAM has converged during the solution process. For instance, Figure 4(a) show the evolution of the value of MD w with the number of cycles when $n_z^1 = 0.33$ and $n_z^2 = 0.61$. The orientation of

individual fractures is randomly allocated and then fracture population are equally divided into two sets in random form in every cycle. Thus Figure 4(a) also show that the value of MD w seem disorganized, yet they still are distributed around a certain value. Figure 4(b) shows that, the average value of the MD v become smooth and constant when the cycles i is larger than 300. So in this configuration, the GBSAM has converged and the maximal cycle number c is equated to 300. Figure 4(c) is an error bar analysis which show that when n_z^2 is from 0 to 1, so that GBSAM has also converged.

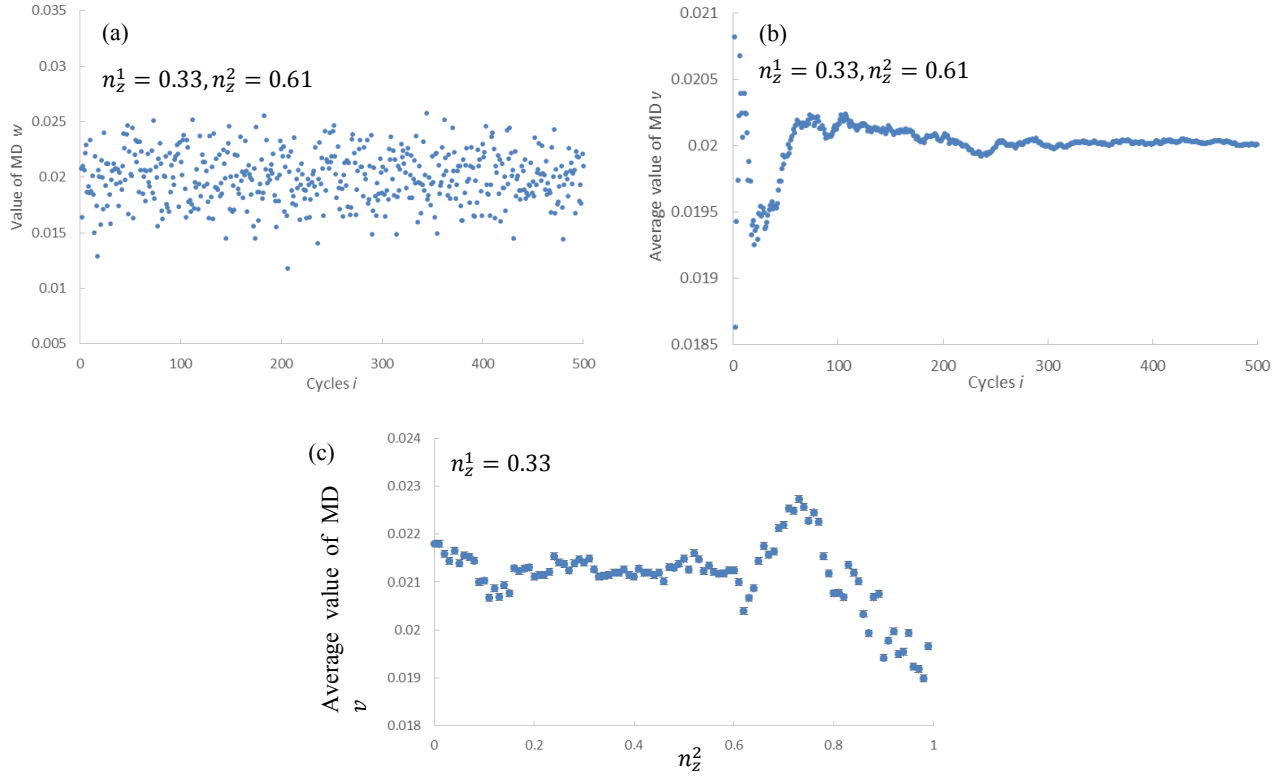

Figure 4: Convergence analysis of GBSAM: (a) the evolution of value of MD with cycles; (b) the evolution of average value of MD with cycles; (c) the error bar analysis for GBSAM.

From above analysis, one needs to select an appropriate maximal cycle number to keep GBSAM converged during the process. For instance, maximal cycle number is equate to 300 which make GBSAM converged under the orientation combination $n_z^1 = 0.33$ and $n_z^2 = 0{\sim}1$. Another check has to be perform under different orientation combinations. In this convergence analysis, the maximal cycle number is 300 making GBSAM converged.

6. NEWBERRY EXAMPLE

In this section, GBSAM is applied to estimate the fractures orientation of Newberry Volcano EGS demonstration, phase 2.1 and 2.2. The stimulated time of Phase 2.1 is 7 weeks and 40000 m3 of water were injected. Phase 2.2 of Newberry EGS stimulation began from September 23, 2014 to November 21, 2014. During this time period, about 2.5 million gallons (9464 m3) of water was injected. A fall-off test was carried out from October 15 to November 10. During phase 2.1 and phase 2.2 stimulation, 494 MEQs were located and recorded (Figure 4(a), (b) and (c)). Borehole tele viewer (BHTV) was installed to map the fractures and 399 fractures were recorded (Figure 6(a)). From the Figure 6(a), the dips of fracture planes are nearly 60^o. The mean value of the dip angles is 57^o and the standard deviation is 18.5^o.

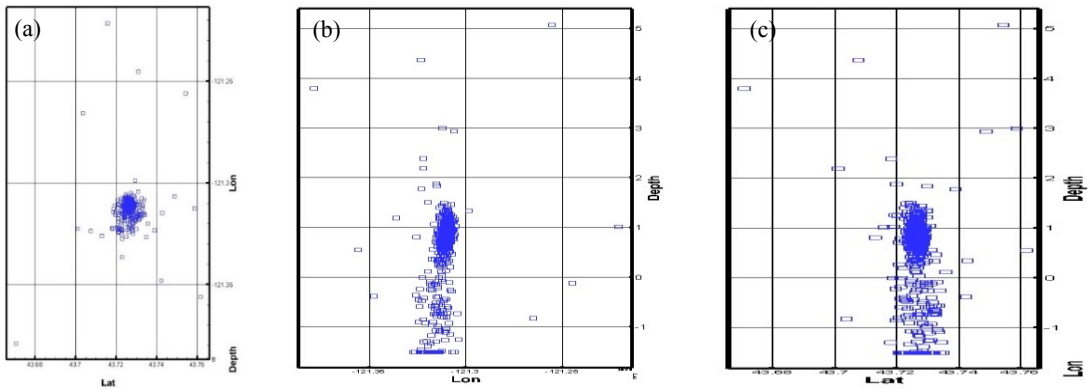

Figure 5: (a) the Lat-Lon view of TMEQs; (b) the Lon-depth (km below sea level) view of TMEQs and (c) Lat-depth (km below sea level) view of MEQs

In this study, we use a line source of length almost equal to half the length of the open hole section of well NWG 55-29, having the same average inject rate $Q = \frac{0.045m^3}{s}$. The length of open section of well NWG 55-29 is 906 m. The reservoir properties in GBSAM used are shown in Table 1. The permeability used is estimated value for the John Day formation(Cladouhos, Petty et al. 2015). In order to simplify the analysis, GBSAM only predicate the normal direction of fracture orientation n_z^1 and n_z^2.

Table 1. Parameters for GBSAM

Parameter	Variable	Value and unit
Vertical Stress (z direction)	σ_z	$55MPa$
Maximum Horizontal Stress(x direction)	σ_x	36 MPa
Minimum Horizontal Stress(y direction)	σ_y	25 MPa
Injection time	t	58 $days$
Injection rate	Q	$0.0045m^3/s$
Biot coefficient	α	0.45
Undrained Poisson's ratio	v_u	0.45
Shear modulus	μ	$25GPa$
Drained Poisson's ratio	v	0.2
Fluid Viscosity	η	$0.85 \cdot 10^{-4} Pa \cdot s$
Permeability	k	$0.072 \cdot 10^{-15}\ m^2$
Hydraulic diffusivity	c	$21.13 \cdot 10^{-2}\ m^2/s$
Cohesive strength	τ_0	0 Pa
Friction coefficient	mu	0.5
Total number of cycles		300
Permeability zone of thickness	$2h$	$400m$

The results from the GBSAM show that the fracture orientation of set 1 is $\{n_x^1, n_y^1, n_z^1\} = \{0.1, 0.89, 0.45\} = \{84^o, 27^o, 63^o\}$ and the fracture orientation of set 2 is $\{n_x^2, n_y^2, n_z^2\} = \{0.1, 0.82, 0.56\} = \{84^o, 35^o, 56^o\}$. The mean and standard deviation of dip angles of fracture is 57o and 18.5o from the BHTV observations. The dip angles from GBSAM are closed to 57o. Here, we need to point that the GBSAM capture the mean of dip angles not entire fracture population because fracture set is assumed to the same orientation. Thus Figure 6(a) shows that the results from GBSAM are in good agreement with observations from BHTV. More than 484 fractures are

sliding. The stored shear strain energy of 165 slipped fractures are larger than threshold energy of MEQs. So the total number of GMEQs is 649. From Figure 6(b)-(d), 484 GMEQs and TMEQs have the same location. So GMEQs has a good match with TMEQs.

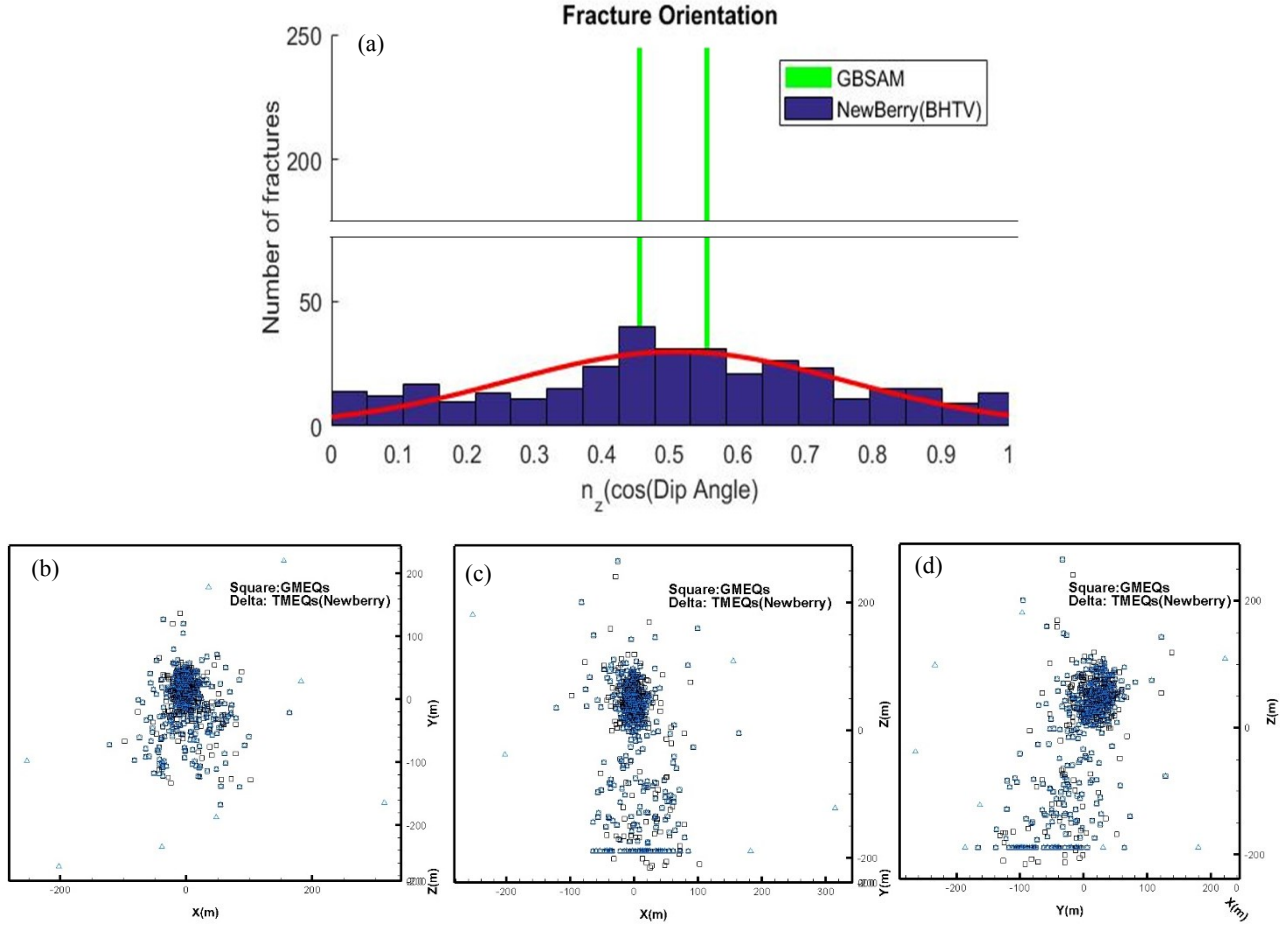

Figure 6: (a) is the comparison between fracture orientation from GBSAM and fracture orientation from BHTV. (b)~ (d) is the map view of GMEQ and TMEQs

7. CONCLUSIONS

In this study, a simple, convergent, and computationally inexpensive method of inverse analysis is proposed to integrate TMEQs and GMEQs to predicate natural fracture orientation in the reservoir. Line source model is used to calculate the distribution of pore pressure used for determination of GMEQs based on fracture slip analysis. If the stored strain energy is larger than threshold energy of MEQs, multiple GMEQs are generated. This assumption can mitigate mesh-dependency issues when simulating MEQs. The fundamental steps in GBSAM is handling discrete data set of MEQs and quantifying a measure of similarity between the GMEQs and TMEQs. This is achieved via MD which is a real value function that quantifies the match between two objects. Convergence analysis shows that GBSAM converges during the processes. Those attractive features of MD makes the GBSAM much better than current MEQs interpretation methods. Finally, GBSAM has been applied to estimate the fracture orientation of Newberry Volcano EGS Demonstration project. Results from GBSAM show that there are two sets of fractures in Newberry reservoirs with dips 63^o and 56^o. The dips of these fractures are in good agreement with the field results from BHTV. In the framework of GBSAM, permeability and stimulate reservoir volume and fracture mechanics properties can be extracted from MEQs. This proposed method provides an effective and general way for interpreting MEQs for better characterizing the reservoir stimulation.

REFERENCES

Aster, R. C. and J. Scott.: Comprehensive characterization of waveform similarity in microearthquake data sets, BULLETIN-SEISMOLOGICAL SOCIETY OF AMERICA **83,** (1993),1307-1307.

Berrone, S., et al.: A Parallel Solver for Large Scale DFN Flow Simulations, SIAM Journal on Scientific Computing, **37**(3), (2015), C285-C306.

Boatwright, J. and J. B. Fletcher.: The partition of radiated energy between P and S waves, Bulletin of the Seismological Society of America, **74**(2), (1984), 361-376.

Brady, J. L., et al.: Microseismic Monitoring of Hydraulic Fractures in Prudhoe Bay, Society of Petroleum Engineers, (1994), SPE-28553-MS

Cha, S.-H.: Comprehensive survey on distance/similarity measures between probability density functions, City **1**(2), (2007), 1.

Cheng, Q. and A. Ghassemi.: Numerical Modeling of Newberry Egs Stimulation, American Rock Mechanics Association, (2016), ARMA-2016-069

Cladouhos, T. T., et al.: Newberry EGS Demonstration: Phase 2.2 Report, ; AltaRock Energy, Seattle, WA (United States)**:** Medium: ED; Size: 138 p. (2015)

Einstein, H. H. and G. B. Baecher. :Probabilistic and statistical methods in engineering geology, Rock mechanics and rock engineering **16**(1), (1983), 39-72.

Farmahini-Farahani, M. and A. Ghassemi.: Analysis of Fracture Network Response to Fluid Injection, Proc. 40th Workshop on Geothermal Reservoir Engineering, (2015)

Fehler, M.:Identifying the plane of slip for a fault plane solution from clustering of locations of nearby earthquakes, Geophysical Research Letters, **17**(7), (1990), 969-972.

Fehler, M., et al.:Determining planes along which earthquakes occur: Method and application to earthquakes accompanying hydraulic fracturing, Journal of Geophysical Research: Solid Earth, **92**(B9) ,(1987), 9407-9414.

Fehler, M. and P. Johnson. :Determination of fault planes at Coalinga, California, by analysis of patterns in aftershock locations, Journal of Geophysical Research: Solid Earth, **94**(B6) ,(1989),7496-7506.

Foulger, G. R., et al.. :Non-double-couple microearthquakes at Long Valley caldera, California, provide evidence for hydraulic fracturing, Journal of Volcanology and Geothermal Research, **132**(1), (2004), 45-71.

Frey, B. J. and D. Dueck. :Clustering by passing messages between data points, science, **315**(5814) ,(2007), 972-976.

Ghassemi, A.:Analysis of Geothermal Reservoir Stimulation using Geomechanics-Based Stochastic Analysis of Injection-Induced Seismicity, Retrieved 02/03, 2017, (2012).

Ghassemi, A.:Analysis of Geothermal Reservoir Stimulation using Geomechanics-Based Stochastic Analysis of Injection-Induced Seismicity, Retrieved 02/03, 2017,(2013).

Ghassemi, A. and Q. Tao. :Thermo-poroelastic effects on reservoir seismicity and permeability change, Geothermics, **63,** (2016), 210-224.

Goodfellow, S. D. and R. P. Young. :A laboratory acoustic emission experiment under in situ conditions, Geophysical Research Letters, **41**(10), (2014), 3422-3430.

Gutierrez-Negrin, L. C. and J. L. Quijano-Leon. :Analysis of seismicity in the Los Humeros, Mexico, geothermal field, Geothermal Resources Council Transactions, **28,** (2003), 467-472.

Huberty, C. J.:Mahalanobis Distance, Encyclopedia of Statistics in Behavioral Science, John Wiley & Sons, Ltd, (2005)

Ishibashi, T., et al.:Linking microearthquakes to fracture permeability change: The role of surface roughness, Geophysical Research Letters ,**43**(14), (2016), 7486-7493.

Jarvis, R. A. and E. A. Patrick. :Clustering using a similarity measure based on shared near neighbors, IEEE Transactions on computers, **100**(11) ,(1973), 1025-1034.

Jones, R. H. and R. C. Stewart. :A method for determining significant structures in a cloud of earthquakes, Journal of Geophysical Research: Solid Earth, **102**(B4), (1997), 8245-8254.

Khazaei, C., et al.:Discrete Element Modeling of Stick-Slip Instability and Induced Microseismicity, Pure and Applied Geophysics, **173**(3) ,(2016), 775-794.

Kuang, W., et al.:Estimating geomechanical parameters from microseismic plane focal mechanisms recorded during multistage hydraulic fracturing, GEOPHYSICS, **82**(1), (2017), KS1-KS11.

Leung, C. T. O. and R. W. Zimmerman. :Estimating the Hydraulic Conductivity of Two-Dimensional Fracture Networks Using Network Geometric Properties, Transport in Porous Media, **93**(3), (2012), 777-797.

Li, S., et al.. :ISRM suggested method for rock fractures observations using a borehole digital optical televiewer, Rock mechanics and rock engineering, **46**(3) ,(2013), 635-644.

Lu, J. and A. Ghassemi.:Geomechanics-Based Stochastic Analysis of Microseismicity for Analysis of Fractured Reservoir Stimulation, (2017)

Pearson, C.:The relationship between microseismicity and high pore pressures during hydraulic stimulation experiments in low permeability granitic rocks, Journal of Geophysical Research: Solid Earth, **86**(B9), (1981),7855-7864.

Pine, R. J. and A. S. Batchelor. :Downward migration of shearing in jointed rock during hydraulic injections, International Journal of Rock Mechanics and Mining Sciences & Geomechanics Abstracts, **21**(5), (1984), 249-263.

Roff, A., et al.:Joint structures determined by clustering microearthquakes using waveform amplitude ratios, International Journal of Rock Mechanics and Mining Sciences & Geomechanics Abstracts, **33**(6), (1996), 627-639.

Safari, R. and A. Ghassemi. :Three-dimensional poroelastic modeling of injection induced permeability enhancement and microseismicity, International Journal of Rock Mechanics and Mining Sciences **84,** (2016), 47-58.

Shapiro, S. A., et al.:Estimating the crust permeability from fluid-injection-induced seismic emission at the KTB site, Geophysical Journal International, **131**(2) ,(1997), F15-F18.

Shapiro, S. A., et al.:Triggering of Seismicity by Pore-pressure Perturbations: Permeability-related Signatures of the Phenomenon, Pure and Applied Geophysics, **160**(5) , (2003), 1051-1066.

Talebi, S., et al.:Microseismic Mapping of a Hydraulic Fracture, American Rock Mechanics Association, (1991).

Tarrahi, M. and B. Jafarpour. :Inference of permeability distribution from injection-induced discrete microseismic events with kernel density estimation and ensemble Kalman filter, Water Resources Research, **48**(10), (2012), n/a-n/a.

Tarrahi, M., et al.. :Integration of microseismic monitoring data into coupled flow and geomechanical models with ensemble Kalman filter, Water Resources Research, **51**(7), (2015), 5177-5197.

Warpinski, N. R., et al.:Analysis and Prediction of Microseismicity Induced by Hydraulic Fracturing, (2004)

Warpinski, N. R., et al.. :Microseismic Monitoring of the B-Sand Hydraulic-Fracture Experiment at the DOE/GRI Multisite Project, (1999)

Williams, J. H. and C. D. Johnson. :Acoustic and optical borehole-wall imaging for fractured-rock aquifer studies, Journal of Applied Geophysics, **55**(1–2) ,(2004), 151-159.

Zhao, X. and R. Paul Young. :Numerical modeling of seismicity induced by fluid injection in naturally fractured reservoirs, GEOPHYSICS, **76**(6) ,(2011), WC167-WC180.